A Nonlinear Derivative Scheme Applied to Edge Detection

Olivier Laligant and Frédéric Truchetet, *Member*, *IEEE*

Abstract—This paper presents a nonlinear derivative approach to addressing the problem of discrete edge detection. This edge detection scheme is based on the nonlinear combination of two polarized derivatives. Its main property is a favorable signal-to-noise ratio (SNR) at a very low computation cost and without any regularization. A 2D extension of the method is presented and the benefits of the 2D localization are discussed. The performance of the localization and SNR are compared to that obtained using classical edge detection schemes. Tests of the regularized versions and a theoretical estimation of the SNR improvement complete this work.

Index Terms—Edge detection, regularization filter, edge localization, edge model, neighbor edge, discrete approach, nonlinear derivative, noises, performance measure.

1 Introduction

Edge detection is one of the oldest topics in image processing and has been widely studied. Methods of edge detection have involved derivative masks, primarily developed in the discrete case, and have been confined to slightly noisy images [1], [2], [3]. The regularization or smoothing [4] and optimal approaches of Canny [5] have led to several efficient continuous operators for noisy and blurred images [6], [7], [8], [9], [10]. Other advanced methods that consider the Canny criterion have been developed to deal with noise, uneven illumination, and image contrast [11]. In a marginal way, discrete approaches for regularization have been developed and have improved results by considering the discrete nature of the images [12], [13].

In the derivative approach, the Canny criteria show how performance is linked to the regularization filter. Increasing regularization improves the SNR at the expense of localization. The regularization filter allows modulation of the balance between these two activities. Thus, linear filtering is well known in the continuous case and, more recently, in the discrete case [14]. Nevertheless, while regularization improves SNR and localization against noise, it often disturbs the geometrical definition and localization of the original edges in the image. Aside from the influence of noise, two close edges can be delocalized by the mutual influence induced by the regularization process [15]. Only specific regularization functions permit edge detection without delocalization due to this mutual influence. Unfortunately, the smoothing ability of these functions is weak (exponentially decreasing around the center of the function). Thus, linear regularization power is bounded with respect to these considerations on close edges (and corners).

• *The authors are with the Le2i Lab., CNRS UMR5158, Université de Bourgogne, IUT, 12 rue de la Fonderie, 71200 Le Creusot, France. E-mail: {olivier.laligant, f.truchetet}@u-bourgogne.fr.*

Manuscript received 18 Jan. 2008; revised 24 July 2008; accepted 10 Nov. 2008; published online 21 Nov. 2008.
Recommended for acceptance by M.-H. Yang.
For information on obtaining reprints of this article, please send e-mail to: tpami@computer.org, and reference IEEECS Log Number TPAMI-2008-01-0038.
Digital Object Identifier no. 10.1109/TPAMI.2008.282.

Introducing nonlinearity into the global filtering process, as in noisy edge detection, is a marginal yet efficient method of obtaining good performance. Generally, nonlinear filtering is used in a preliminary regularization stage. Pitas and Venetsanopoulos [16] propose a class of nonlinear filters that rejects additive and impulse noise, while preserving the edges. More recently, Benazza-Benyahia et al. [17] introduced a nonlinear filter bank leading to a multiresolution approximation of the signal in which discontinuities are well preserved. A nonlinear filter for edge enhancement, using a morphological filter, has been proposed by Schulze [18]. Here, the author shows that local variation analysis allows to enhance edges corrupted by multiplicative noise. Hwang and Haddad [19] present an integrated nonlinear edge-detection-based denoising scheme. A thresholded derivative is computed from two half filters (median for impulse noise, mean for Gaussian noise, and min-max for uniform noise) and edge detection is used to select the second filtering stage, i.e., mean for noise or median for edge points. In this scheme, edge detection could be considered as a by-product and the optimal performance is obtained only when the correct first filter is selected according to the noise statistic. It must also be noted that a minimum window size of six samples is required.

In this work, we propose to obtain both noise reduction and edge detection by a one-stage nonlinear derivative scheme. This scheme, which consists of combining two polarized differences, yields significant improvements in SNR without using regularization or increasing the computational requirements.

Section 2 revisits edge detection using a derivative approach and discrete edge localization. Section 3 introduces the 1D principle of the method and its 2D extension. Section 4 focuses on the properties of the proposed scheme and Section 5 presents the performances of the method on synthetic and real images. A short study of regularized versions of the method is also introduced. Section 6 deals with natural images. Finally, a conclusion and an appendix complete the paper.

Note that all images (before eventually adding the noise) in this work are normalized to 1.

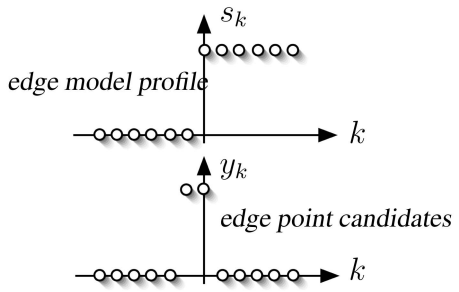

Fig. 1. Discrete model for edge-profile and edge-point candidates.

2 Discrete Edge Detection and Localization Problem

2.1 Edge Detection by Derivative Approach

Let us review some of the basics of edge detection using a derivative approach. The classical continuous model of edge detection involves the Heaviside function: $C(x) = H(x)$. Edge detection corresponds to gradient computing and is achieved by two directional filtering operations, regularized by a low-pass filter h or not ($h = \delta$) [4]:

$$\overrightarrow{g(x,y)} = \begin{pmatrix} \frac{\partial}{\partial x} h * I(x,y) \\ \frac{\partial}{\partial y} h * I(x,y) \end{pmatrix} = \begin{pmatrix} f_x * I(x,y) \\ f_y * I(x,y) \end{pmatrix} = \begin{pmatrix} g_x(x,y) \\ g_y(x,y) \end{pmatrix}, \tag{1}$$

where $I(x,y)$ is the original image and $f_x(x,y)$ and $f_y(x,y)$ are the directional regularized detectors. When $h(x,y)$ is separable, $f_x(x,y) = f(x)h(y)$ and $f_y(x,y) = h(x)f(y)$.

From the gradient images, the gradient modulus and edge orientation images are calculated, followed by the local maxima of the image. Finally, a segmentation stage (for example, a simple thresholding process) leads to the representation of the edges in the image.

In the optimal approaches developed for the continuous case, the filters are finally transposed to the discrete case by a simple sampling; however, sampling the edge model induces a technical problem for edge localization. This problem must be considered when evaluating the performance of the method [14], [20].

2.2 Discrete Edge Model and Localization

Let us consider high contrast or synthetic images. According to the model of an ideal step edge, two points on both sides of the transition are edge-point candidates (see Fig. 1). The ideal edge point would be, in fact, between two pixels (subpixel detection [13]).

Usually, one maximum is selected from the two points. Such a condition yields the local maxima extraction:

$$|g_{\text{neighbor in the gradient direction}}| < |g| \leq |g_{\text{neighbor in the inverse gradient direction}}|.$$

The role of the asymmetry in this condition is particularly obvious in the case of synthetic images. Nevertheless, for noisy images, asymmetry induces an ambivalent local maxima representation both in synthetic images and in real sharp images. This effect is particularly observed on straight lines (see Fig. 8d). Moreover, choosing one particular edge-point candidate implies that a change in the sign of the step edge induces a different localization result (see Fig. 2). In the images, this leads to a poor localization at the corners of the objects (see image in Fig 5a and detection in Fig. 5b).

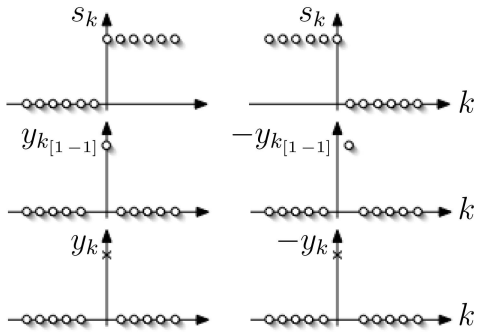

Fig. 2. The edge localization varies ($y_{k_{[1\ -1]}}$) according to the sign of the transition (detector $[1\ \ -1]$). Below, we will choose (see Section 3) the localization represented by the cross.

We propose a new scheme to solve these problems of delocalization and improve the SNR of the edge image. We use a regular sampling grid and do not consider subpixel and/or interpolated localization [21].

3 Nonlinear Filtering Scheme for Edge Localization

We first introduce the 1D principle before proposing an extension to 2D. A comment on the ability of the new scheme, in terms of localization, will conclude this section. We will denote the proposed *nonlinear filtering scheme* by NLFS.

3.1 1D Principle of NLFS

Fig. 3 presents the configuration of two opposite profiles. We propose to localize the edge point according to the sign of the slope of the transition. If this slope is positive, the point will be validated after the transition; if the slope is negative, it will be validated before.

In this way, we introduce two detector filters, F_+ and F_-, regularized or not, without 0 at their centers, as

$$F_-(z) = -F_+(z^{-1}). \tag{2}$$

Responses are selected using a nonlinear operator T as a threshold. Two signals are obtained: Y_+, containing positive-slope edge points, and Y_-, containing negative-slope edge points:

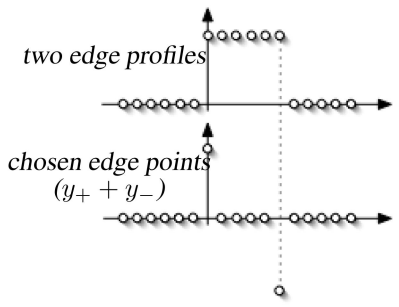

Fig. 3. NLFS localization for discrete edge detection.

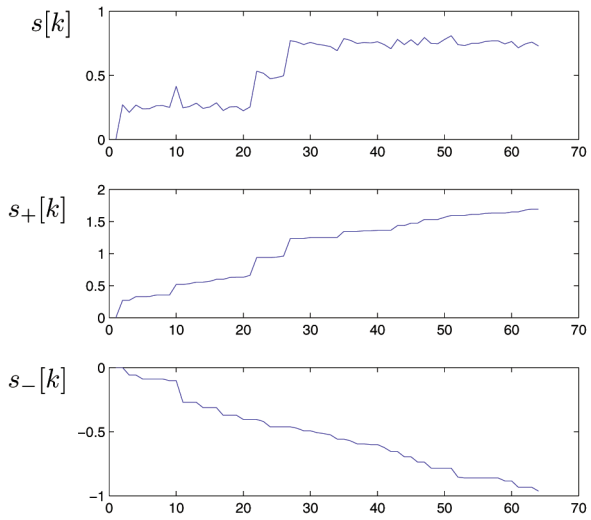

Fig. 4. Signal interpretation: directional signal decompositions.

$$\begin{cases} Y_+(z) = T(F_+(z)S(z)), \\ Y_-(z) = -T(-F_-(z)S(z)). \end{cases} \tag{3}$$

Similar definitions have been used by Chen [22] to characterize local discontinuities. In Fig. 3, the sum of the two signals y_+ and y_- corresponds to the illustration.

The original signal s can be seen as two signals s_+ and s_- containing positive ($s_+[k] = s_+[k-1] + y_+[k]$) and negative ($s_-[k] = s_-[k-1] + y_-[k-1]$) variations (Fig. 4). Generally (except for particular filters like $[1\ \ -1]$),

$$s[k] \neq s_+[k] + s_-[k]. \tag{4}$$

Another interpretation of this approach could be as follows: A derivative filtering of the signal is performed in both directions, from left to right and from right to left. For each direction, only variations with the same sign are retained (see Fig. 4). Due to this interpretation, the choice of the maximum, according to the direction, is always the same. Let us finally note that, from the perspective of algorithmic cost and for symmetric negative and positive filter parts, a single filter is sufficient for memorizing the operations relating to the pixel closest to the current pixel (no additional computational cost). Relation 2 can be written as $F_-(z) = zF_+(z)$ for these filters.

In slightly noisy images, which is a common situation in real images, the disturbances caused by the noise appear as isolated peaks. These peaks are detected by y_+ and y_- at the same location and are therefore erased. A "natural" noise reduction is thus obtained with no penalty in terms of computational cost (no regularization filter is necessary).

3.2 2D Extension

Extension of this algorithm to 2D or higher dimensions is achieved in a separable way by introducing the polarized gradients G_+ and G_-:

$$G_+ = \begin{pmatrix} G_{x+} \\ G_{y+} \end{pmatrix} = \begin{pmatrix} T(F_+(z)I(z,.)) \\ T(F_+(z)I(.,z)) \end{pmatrix}, \tag{5}$$

$$G_- = \begin{pmatrix} G_{x-} \\ G_{y-} \end{pmatrix} = \begin{pmatrix} -T(-F_-(z)I(z,.)) \\ -T(-F_-(z)I(.,z)) \end{pmatrix}. \tag{6}$$

From the polarized gradient images, an edge detection modulus can be obtained as follows ($G = \mathbf{Z}[g]$):

$$|g| = \sqrt{(g_{x+} + g_{x-})^2 + (g_{y+} + g_{y-})^2}. \tag{7}$$

4 Properties of the Basic NLFS Scheme

4.1 Reference Derivative Schemes for Comparison

Since this scheme is nonlinear, some properties will depend on the choice of $F_{+/-}$. In this paper, we will choose the basic filter (and for some parts, we will also choose a regularization) and compare its properties to the basic definition of the discrete derivative (no regularization) and the fundamental linear scheme used for edge detection. The nonlinear operator T is the simple threshold: $T(x) = x$ if $x \geq 0$, 0 elsewhere. We define the following:

- The NLFS with $F_+(z) = -z^{-1} + 1$.
- The classical scheme without a 0 at the center (CFS): $-z^{-1} + 1$. This corresponds to the simplest definition of the discrete derivative.
- The regularized classical scheme with a 0 at the center (CFS0): $(-z^{-1} + 0 + z)/2$. This corresponds to regularized filters, such as the Canny, Canny-Deriche, and Shen & Castan detectors. Indeed, these filters usually have 0 at the center. Note that the 0 at the center in the basic operator already induces a (small) regularization of $(1+z)/2$. To estimate the components of the gradient in images, the regularization ($(1+z)/2$) is performed along the lines (the columns) while the regularized detection ($(-z^{-1} + 0 + z)/2$) is performed along the columns (the lines).

4.2 Rotational Invariance of Localization

It is known that an antisymmetric linear (derivative) filter (no 0 value at the center) gives a shifted pixel localization and this localization changes depending on edge orientation. Since the NLFS considers the orientation of the edge profile (the sign of the variation), it provides univocal localization; this localization only depends on the profile (variation). We thus have:

$$Y(z) = Y_+(z) + Y_-(z) \tag{8}$$

$$= T[F_+(z)S(z)] - T[-F_-(z)S(z)]. \tag{9}$$

For a symmetric signal $S^r(z) = S(z^{-1})$, the response is:

$$Y^r(z) = Y^r_+(z) + Y^r_-(z) \tag{10}$$

$$= T[F_+(z)S^r(z)] - T[-F_-(z)S^r(z)] \tag{11}$$

$$= T[-F_-(z^{-1})S(z^{-1})] - T[F_+(z^{-1})S(z^{-1})] \tag{12}$$

$$= -Y_-(z^{-1}) - Y_+(z^{-1}), \tag{13}$$

leading to

$$\begin{cases} y^r_{+,k} = -y_{-,-k} \\ y^r_{-,k} = -y_{+,-k} \end{cases} \tag{14}$$

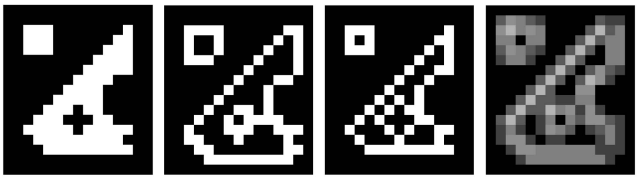

(a) (b) (c) (d)

Fig. 5. Edge detection (modulus) on a synthetic image: (a) original image, (b) CFS detection, (c) NLFS, and (d) CFS0 (regularized). In (c), edge points are detected inside the pattern. Edge points are shifted in (b) and thick in (d), and then are sensitive to noise.

and

$$y_k^r = -y_{-k.} \tag{15}$$

While the response is polarized (the sign depends on the orientation), the localization is unchanged. The 2D extension inherits this property. Fig. 5c demonstrates this result.

This property is still valid for filters that lack symmetry. This NLFS scheme could be useful for wavelet analysis with nonlinear phase wavelets.

4.3 Edge Pixel Localization on Synthetic Images

Fig. 5 exemplifies the difficulties of edge localization for a synthetic image. Notably, the suggested method localizes the edges inside the frontier of the form. The traditional method, without regularization (CFS), gives a representation of edges that are shifted in a particular direction. The regularized version (with a 0: CFS0) gives thick edges; however, any presence of noise makes this representation very chaotic.

Changing the localization of edges (to outside the frontier of the form) is possible with a simple shift of the detectors. Depending on the selected localization and the object luminance (and background), the edges will always be detected inside or outside the form. This is an interesting property for dimensional control (non-subpixel localization), given that the localization is defined in a univocal way.

4.4 Signal-to-Noise Ratio

Since the NLFS is nonlinear, its effect has to be considered in both the signal and noise. In this section, after some definitions, the response of the NLFS to the classical edge model is estimated in the presence of Gaussian white noise. The estimation of the NLFS effect on the noise then provides an indication of the theoretical performance of the NLFS. A complete demonstration of these results is proposed in the Appendix.

4.4.1 Signals Definition

Let us consider the noisy signal s_k:

$$s_k = A.H_k + n_k, \tag{16}$$

where

$$H_k = 1 \quad \text{if } k \geq 0, \quad 0 \text{ elsewhere}, \tag{17}$$

and n_k is an outcome of the stochastic variable $\mathcal{N}_k$ denoting a Gaussian white noise with 0 mean and σ standard deviation.

4.4.2 Signal Output

Applying the NLFS to the signal s_k with the filter $f_+ = [\underline{1} \ -1]$, we obtain the response $y = y_+ + y_-$:

$$\begin{cases} y_{+,k} = T[s_k - s_{k-1}], \\ y_{-,k} = -T[-(s_{k+1} - s_k)]. \end{cases} \tag{18}$$

At $k = 0$ and introducing the noise and the edge model,

$$\begin{cases} y_{+,0} = T[(A + n_0) - (0 + n_{-1})], \\ y_{-,0} = -T[-((A + n_1) - (A + n_0))], \end{cases} \tag{19}$$

and then,

$$y_0 = T[A + n_0 - n_{-1})] - T[-n_1 + n_0]. \tag{20}$$

In the following, the noise level should be weak compared to the amplitude A ($\sigma \ll A$). If this is not the case, the effect of the threshold will depend on the amplitude A and experimental results show that the properties are close to those of the classical schemes (see Fig. 9). It follows from the calculations in the Appendix that the energy $E\{\mathcal{Y}_0^2\}$ of the random process $\mathcal{Y}_0$, where the outcomes are y_0, is

$$E\{\mathcal{Y}_0^2\} = A^2 - A.\frac{2}{\sqrt{\pi}}.\sigma + 2\sigma^2 \quad \text{if } \sigma \ll A. \tag{21}$$

These results show that the NLFS has a tendency to attenuate the edge response under the influence of noise. The amplitude of the signal depends on the noise level.

4.4.3 Noise Output

For the noise component, the detection leads to

$$\begin{cases} y_{+,k} = T[s_k - s_{k-1}], \\ y_{-,k} = -T[-(s_{k+1} - s_k)], \end{cases} \tag{22}$$

or (for $k \neq \{-1, 0, 1\}$):

$$\begin{cases} y_{+,k} = T[n_k - n_{k-1}], \\ y_{-,k} = -T[-(n_{k+1} - n_k)]. \end{cases} \tag{23}$$

Developing the different cases (see the Appendix), we finally obtain:

$$E\{Y_k\} = 0, \tag{24}$$

$$E\{Y_k^2\} = \frac{\pi}{4}\sigma^2, \tag{25}$$

$$\approx 0.785\sigma^2. \tag{26}$$

This means that, while a derivative operation is performed, the variance σ^2 of the centered noise is reduced to $0.785\sigma^2$ (the noise stays centered).

4.4.4 Theoretical SNR

The theoretical SNR is defined by:

$$SNR = \frac{\text{signal power average}}{\text{noise power average}} \tag{27}$$

$$= \frac{\text{noisy signal power average} - \text{noise power average}}{\text{noise power average}}, \tag{28}$$

with the previous results:

$$SNR = \frac{\left(A^2 - A \cdot \frac{2}{\sqrt{\pi}} \cdot \sigma + 2\sigma^2\right) - \frac{\pi}{4}\sigma^2}{\frac{\pi}{4}\sigma^2} \tag{29}$$

$$= \frac{4}{\pi} \cdot \frac{A^2}{\sigma^2} \left(1 - \frac{2}{\sqrt{\pi}} \cdot \frac{\sigma}{A} + \frac{8-\pi}{4} \cdot \frac{\sigma^2}{A^2} \right). \quad (30)$$

Seeing the condition for the signal power average evaluation ($\sigma \ll A$), we have $\frac{2}{\sqrt{\pi}} \cdot \frac{\sigma}{A} \gg \frac{8-\pi}{4} \cdot \frac{\sigma^2}{A^2}$ and

$$SNR \approx \frac{4}{\pi} \cdot \frac{A^2}{\sigma^2} \left(1 - \frac{2}{\sqrt{\pi}} \cdot \frac{\sigma}{A} \right), \quad (31)$$

and then

$$SNR_{\max} \approx \frac{4}{\pi} \cdot \frac{A^2}{\sigma^2} \quad (32)$$

$$\approx 1.27 \frac{A^2}{\sigma^2}. \quad (33)$$

4.4.5 Comparison with the Theoretical SNR for the Classical Scheme

$$SNR_{CFS,CFS0} = \frac{1}{2} \cdot \frac{A^2}{\sigma^2}. \quad (34)$$

We can now establish the gain of the basic NLFS scheme in terms of the SNR:

$$G_{SNR} = \frac{8}{\pi} \left(1 - \frac{2}{\sqrt{\pi}} \cdot \frac{\sigma}{A} \right) \quad \text{if } \sigma \ll A \quad (35)$$

and the maximum gain:

$$G_{SNR\max} = \frac{8}{\pi} \quad \text{if } \sigma \ll A \quad (36)$$

$$\approx 2.55. \quad (37)$$

As NLFS output depends on three samples (s_{k-1}, s_k, s_{k+1}), a fair comparison would be to employ a linear 3-tap filter: this is the case of CFS0 (in 1D).

The basic NLFS offers a good gain in SNR without any regularization. For noise reduction, the result of the NLFS scheme is equivalent to the following regularized (linear) filter (see Fig. 6):

$$f[k]_{k\in[-3;4]} = [0.0350 \quad 0.0983 \quad 0.3778 \quad 0.4889 \quad -0.4889 \quad -0.3778 \quad -0.0983 \quad -0.0350]$$

with:

$$\sum_{k=-3}^{0} f[k] = 1, \quad (38)$$

$$\sum_{k=-3}^{4} f[k]^2 = 0.785. \quad (39)$$

If we consider the optimal filter for SNR (difference of boxes, see [5], [14]): the filter

$$[0.3333 \quad 0.3333 \quad 0.3333 \quad -0.3333 \quad -0.3333 \quad -0.3333],$$

the noise is reduced by the coefficient $\sum_{k=-3}^{4} f[k]^2 = 0.666$. This means that the minimum width (number of coefficients) of the regularized equivalent filter is at least 6. Note the particular normalization ($\sum_{k=-3}^{0} f[k] = 1$ instead of $\sum_{k=-3}^{4} h[k] = 1$) for this comparison.

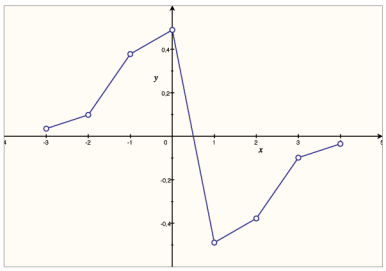

Fig. 6. An equivalent linear filter (from the noise reducing point of view) $\sum_{k=-3}^{4} f[k]^2 = 0.785$. Note the particular normalization here $\sum_{k=-3}^{0} f[k] = 1$ to obtain the amplitude 1 in response to the step model (in general, h should be normalized to 1 with $f = \frac{dh}{dx}$).

4.4.6 2D Extension

The energy of the noisy signal for each direction of detection is

$$\begin{cases} E\{\mathcal{Y}_{0x}^2\} \approx A_x^2 - A_x . \frac{2}{\sqrt{\pi}} . \sigma + 2\sigma^2 & \text{if } \sigma \ll A_x, \\ E\{\mathcal{Y}_{0y}^2\} \approx A_y^2 - A_y . \frac{2}{\sqrt{\pi}} . \sigma + 2\sigma^2 & \text{if } \sigma \ll A_y, \end{cases} \quad (40)$$

and then

$$E\{\mathcal{Y}_0^2\} \approx A^2 - (A_x + A_y) . \frac{2}{\sqrt{\pi}} . \sigma + 4\sigma^2 \quad \text{if } \sigma \ll A. \quad (41)$$

For the classical schemes:

$$E\{\mathcal{Y}_0^2\}_{CFS} = \left(A_x^2 + 2\sigma^2\right) + \left(A_y^2 + 2\sigma^2\right) \quad (42)$$

$$= A^2 + 4\sigma^2, \quad (43)$$

$$E\{\mathcal{Y}_0^2\}_{CFS0} = \left[\left(\frac{A_x}{2} \right)^2 + \frac{\frac{\sigma^2}{2^2}}{\frac{2^2}{2^2}} \right] + \left[\left(\frac{A_y}{2} \right)^2 + \frac{\frac{\sigma^2}{2^2}}{\frac{2^2}{2^2}} \right] \quad (44)$$

$$= \frac{A^2}{4} + \frac{\sigma^2}{2}. \quad (45)$$

The SNR is calculated as:

$$SNR_{CFS} = \frac{1}{4} . \frac{A^2}{\sigma^2}, \quad (46)$$

$$SNR_{CFS0} = \frac{1}{2} . \frac{A^2}{\sigma^2}, \quad (47)$$

$$SNR_{NLFS} = \frac{2}{\pi} . \frac{A^2}{\sigma^2} . \left(1 - \frac{A_x + A_y}{A^2} . \frac{2}{\sqrt{\pi}} . \sigma \right) \quad \text{if } \sigma \ll A, \quad (48)$$

and the maximum gains are:

$$G_{SNR_{\max/CFS}} = \frac{8}{\pi} \quad \text{if } \sigma \ll A, \quad (49)$$

$$G_{SNR_{\max/CFS0}} = \frac{4}{\pi} \quad \text{if } \sigma \ll A. \quad (50)$$

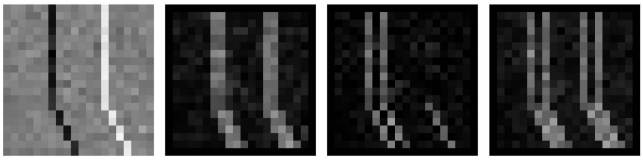

(a) (b) (c) (d)

Fig. 7. Drawback of edge detection (modulus) on a noisy synthetic image: (a) original image + Gaussian white noise ($\sigma^2 = 0.0015$), (b) CFS detection, (c) NLFS, and (d) CFS0. The NLFS does not detect the vertical white line seen as a noise impulse in 1D. Shifting the detectors would cause nondetection of the black lines.

Equations (41) and (48) show that the NLFS will attenuate the detection amplitude for diagonal gradient directions more than for vertical and horizontal directions. The CFS0 has an improved SNR in comparison with the 1D version since a regularization is performed on the two directions to estimate the gradient components.

It can be noted that the number of pixels involved in the linear and nonlinear schemes is different: 3 for CFS, 8 for CFS0, and 5 for NLFS. Therefore, a comparison on this basis is not possible. But (49) and (50) show that the gain of the nonlinear scheme is better in all cases. In Section 5.5, experimental results allowing a fair comparison from this point of view (same neighborhood size) are given.

4.5 Nondetection of Thin Lines

While the NLFS scheme has high localization and good noise cancellation performance, it suffers from its 1D definition in the 2D extension. Indeed, positive impulses are interpreted as noise-inducing. For example, thin, light-gray edge lines ($\text{thickness} = 1$ pixel) are seen as noise. Fig. 7 shows this phenomenon on a noisy synthetic image.

5 Performance of the NLFS Scheme

We first verify the theoretical performance of the algorithm on synthetic images. A simple criterion is then introduced to evaluate and compare the performance of the NLFS to real images. Two regularized versions are then proposed for the NLFS. These schemes are compared to the classical scheme.

Throughout this section, the regularization filter is denoted by h (or $H(z)$) and the NLFS is composed of the two elementary nonregularized filters: $F_+(z) = 1 - z^{-1}$, $F_-(z) = z - 1$.

5.1 Performance on Synthetic Images

5.1.1 1D Localization on Noisy Images

Fig. 8 shows the effect of noise on the localization. Here, the test image corresponds to the Pratt figure of merit [20]. The noise induces a chaotic localization of the edge in the 1D-CFS0 case. This phenomenon often also occurs with noisy real images (processed by CFS0).

Clearly, the 1D NLFS leads to less noisy images than the 1D CFS or 1D CFS0. The next section presents the results obtained in 2D.

5.1.2 SNR on Noisy Synthetic Images

Considering the synthetic image in Fig. 8, we perform the edge detection with the classical derivative scheme CFS and the proposed NLFS. In order to measure the performance, a second edge detection is carried out on the original image added to a Gaussian white noise image of variance σ^2. For low noise levels, the results in Fig. 9 roughly correspond to the theoretical predictions. For higher levels, as previously stated, the results will depend on the noise level and the edge amplitude.

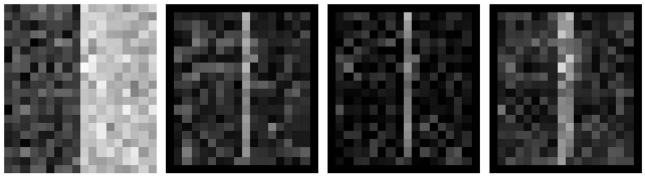

(a) (b) (c) (d)

Fig. 8. 1D edge detection (modulus) on a noisy synthetic image: (a) original image + Gaussian white noise ($\sigma^2 = 0.0015$), (b) CFS detection, (c) NLFS, and (d) CFS0 (no 2D-regularization). The noise level of the NLFS case is clearly lower than those of other cases. Local maxima detection gives a badly localized line with CFS0.

5.2 Performance on Noisy Real Images

5.2.1 Performance Criteria

In this section, we evaluate the performance of the NLFS scheme compared with the standard derivative CFS. Real images cannot be directly used for segmentation and then for performance evaluation; each algorithm produces too different results for localization and amplitude. In order to deal with this difficulty, we define a measurement procedure (summarized in Fig. 10). In order to measure the performance of a detection algorithm:

- Let there be a real image I.
  - A detection is performed with the algorithm that produces the reference image R.
  - A local maxima detection stage leads to the image R_l.
  - Finally, a segmented image R_t is obtained by a simple threshold t_d: if $R_t(i,j) \geq t_d$, $R_t(i,j) = 1$, else 0.

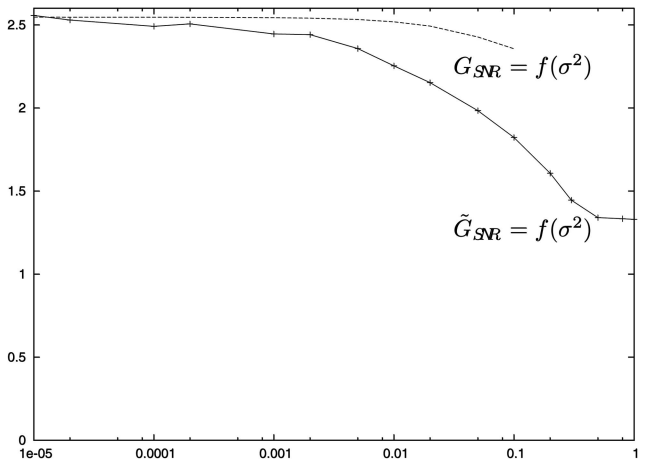

Fig. 9. Estimated $\tilde{G}_{SNR}$ with respect to the Gaussian noise level (variance). Comparison with the theoretical gain G_{SNR}.

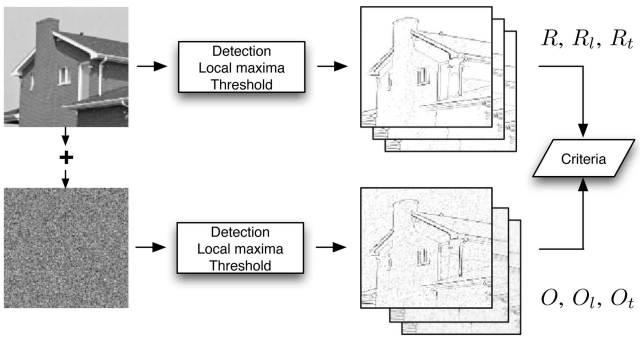

Fig. 10. Procedure for performance evaluation.

- A Gaussian white noise image is generated and added to image I to obtain I_n.
- Steps 1 to 3 are repeated on the new image I_n to produce the outputs O, O_l, and O_t.
- A performance criterion C_p is defined. Let E_R be the set of n_E edge points, where $R_t(i,j) \neq 0$, and $\bar{E}_R$ be the complementary set of $n_{\bar{E}_R}$ nonedge points, where $R_t(i,j) = 0$:

$$C_p = \frac{S_O^2 - N_{O/R}^2}{N_{O/R}^2}, \tag{51}$$

where

$$S_O^2 = \frac{1}{n_{E_R}} . \sum_{i,j \in E_R} O(i,j)^2, \tag{52}$$

$$N_{O/R}^2 = \frac{1}{n_{\bar{E}_R}} . \sum_{i,j \in \bar{E}_R} (O(i,j) - R(i,j))^2. \tag{53}$$

The criterion C_p jointly measures the SNR and localization (due to the maxima detection) of the considered algorithm. This two-stage procedure allows us to observe the relative effects of the algorithm on the noisy image. The bias induced by thresholding the original image is also avoided. This measure is almost independent of the threshold value. By comparing the value ratio of C_p for the two detection algorithms, the result is also independent of the noise level if it is small and sufficient (to be preponderant on the noise in the original image).

When tested on synthetic images, the criterion leads to the following result: $C_{p_{NLFS}}/C_{p_{CFS}} = 2.5$ (for small noise levels), which corresponds to the theoretical ratio in the SNR. In order to measure the performance of the algorithms on real images, we will assume the following:

$$C_p \equiv SNR. \tag{54}$$

5.2.2 Comparison with the Classical Derivative Scheme

Table 1 presents some performance results. The NLFS clearly outperforms the equivalent (for the filter definition) linear scheme (see Fig. 11). The gain decreases for low and high noise levels. For low noise levels, the decay in the performance ratio is due to the criterion definition (the relative added noise level becomes too small). The second case (high noise levels) confirms the theoretical and experimental results on the synthetic images. The results

TABLE 1
Performance of the CFS and NLFS on the Image *House*

σ^2	0.0001	0.0005	0.001	0.005	0.01	0.05
$C_{P_{CFS}}$	207	38	18	3.2	1.6	0.34
$C_{P_{NLFS}}$	317	71	36	7.0	3.5	0.71
ratio	1.5	1.9	2.0	2.2	2.2	2.1

These results (ratio) do not change for a threshold in the range $[0.08; 0.16]$. *Beyond this range, the number of edge points becomes insufficient. As the threshold decreases below 0.08, the performance ratio increases but the resulting images become very noisy.*

(ratio) do not change for a threshold in the range $[0.08; 0.16]$ for the *House* image. Beyond this range, the number of edge points becomes insufficient. As the threshold decreases below 0.08, the performance ratio increases but the resulting images become very noisy. These remarks remain valid for all ensuing experiments.

5.3 Performance with Basic Regularization (Smoothing) on Noisy Real Images

In this section, we define regularized versions of the NLFS and compare their performance to the basic regularization (corresponding to the classical edge detection scheme) carried out by the filter $[1\ \ 1]$, even though the main interest of the NLFS is the gain without using regularization.

5.3.1 A Simplified Real Edge Model

In real images, the projection of a step edge on the sensor does not correspond well to the Heaviside function [8], [23]. The integration pixel surface induces an edge profile C_r that we will model as follows:

$$C_r(k) = \begin{cases} 0 & \text{if } k < 0, \\ (0.5 - x).A & \text{if } k = 0, \\ A & \text{if } k > 0, \end{cases} \tag{55}$$

with A representing the edge amplitude and x $(-0.5 \leq x \leq 0.5)$ the original localization of the projected profile. For a free-noise signal, detection by the NLFS scheme gives:

$$\begin{cases} y_0 = (0.5 - x).A, \\ y_1 = (0.5 + x).A. \end{cases} \tag{56}$$

In this work, we used the detection filter $(z^1 - z^{-1})/2$ ($CFS0$) involving the edge detector $1 - z^{-1}$ and the basic regularization filter $H(z) = (1 + z)/2$; therefore, a general definition of the detection filter $D(z)$ is given by (H being the regularization term)

$$D(z) = (1 - z^{-1}).H(z). \tag{57}$$

The corresponding detection (with $H(z) = (1 + z)/2$) is

$$\begin{cases} y_{-1} = (0.5 - x).A/2, \\ y_0 = A/2, \\ y_1 = (0.5 + x).A/2. \end{cases} \tag{58}$$

5.3.2 Basic Regularization for the NLFS

Equation (56) shows the typical response of the NLFS scheme "inside" (for the chosen definition of the NLFS) the edge profile (y_0 and y_1), while the CFS0 produces a centered response (y_{-1}, y_0, and y_1). In order to induce an equivalent

(a) (b) (c)

Fig. 11. *House* image + Gaussian noise $\sigma^2 = 0.005$ (a). Comparison between CFS and NLFS: the gradient modulus after local maxima and thresholding (0.08). (b) CFS and (c) NLFS.

regularization with the NLFS, the definition of the basic regularization filters (h_+ and h_-) has to be adapted to the components y_+ and y_-:

$$\begin{cases} H_+(z) = \dfrac{z^1 - z^{-1}}{2} \cdot \dfrac{1}{F_+(z)}, \\ H_-(z) = \dfrac{z^1 - z^{-1}}{2} \cdot \dfrac{1}{F_-(z)}, \end{cases} \tag{59}$$

with the two elementary nonregularized filters $F_+(z) = 1 - z^{-1}$, $F_-(z) = z - 1$, and then

$$\begin{cases} H_+(z) = (1+z)/2, \\ H_-(z) = (1+z^{-1})/2. \end{cases} \tag{60}$$

The algorithm dealing with the image I is summarized below:

- smooth image I with H_+ and H_- along the lines and columns to obtain I_+ and I_-;
- perform the 2D component detection G_{x+}, G_{y+} and G_{x-}, G_{y-} on I_+ and I_-, respectively;
- calculate $G_x = G_{x+} + G_{x-}$, $G_y = G_{y+} + G_{y-}$ as previously and, finally, $|\vec{g}|$ and $\arg[\vec{g}]$.

5.3.3 A Second Method of Regularization with the NLFS

Since NLFS is nonlinear, changing the order of the operators will theoretically change the results. A second version for NLFS can be defined (NLFS II). After the detection using the nonregularized filters F_+ and F_-, a regularization is performed. The regularization is unique, as illustrated in Fig. 12. This means that the regularization filter should be symmetrical for images (2D or more); however, a shifted edge representation (as in the simple scheme $[1 \ -1]$) can be obtained with shifted filters (like $[1\ 1]/2$). The smoothing "power" of this filter is equal to $0.5^2 + 0.5^2 = 0.5$. An equivalent filter (from the smoothing point of view) $bz^1 + a + bz^{-1}$ can be defined by:

$$\begin{cases} a + 2b = 1 & \text{norm}, \\ a^2 + 2b^2 = 0.5 & \text{smoothing "power,"} \end{cases} \tag{61}$$

leading to $H(z) = 1/6z^1 + 2/3 + 1/6z^{-1}$.

The number of pixels involved in these nonlinear regularized schemes is 12.

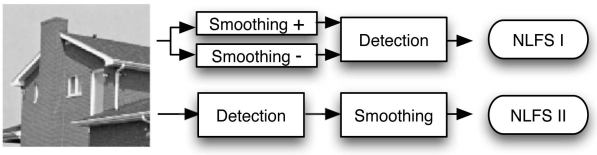

Fig. 12. The two versions for NLFS with regularization.

5.3.4 Comparison of CFS0, NLFS I, and NLFS II

Table 2 presents the results we obtained on the synthetic images. Table 3 presents the performance of the standard NLFS and the nonlinear regularized schemes referenced to the classic scheme $[1 \ -1]$. The CFS0 outperforms the NLFS on segmented real images. This is mainly due to the expanse of the profile (see the edge model in (55)) being better detected in the regularization case; however, the NLFS is similar to the CFS0 in terms of SNR on the detection images (no local maxima). The regularized schemes NLFS I and NLFS II generally outperform the CFS0, regardless of the noise level and the threshold (see Fig. 13). For weak noise, the methods perform similarly, but NLFS I and NLFS II are slightly better. In general, the attenuation tendency on the edge amplitude is weak and can explain the small difference in performance between CFS0 and NLFS I-NLFS II in some cases for very low noise levels. The fine details are generally detected better with the NLFS II, seeing as the regularization is carried out after the derivative operations.

Compared to the nonregularization versions, the performances do not improve proportionally to the regularization "power" ($1/\sum h[k]^2$). According to some experiments, the

TABLE 2
Performance on Synthetic Images
(Noise Level $\ll$ Edge Amplitude)

	$C_{p_{scheme/CFS}}$			
$H(z)$	NLFS	CFS0	NLFS I	NLFS II
$(1+z)/2$	2.5	2.0	2.3	3.0
$1/6z^1 + 2/3 + 1/6z^{-1}$	2.5	3.2	5.4	5.4

CFS0: $D(z) = (1 - z^{-1}).H(z)$.

TABLE 3
Performance of the Standard NLFS and the Regularized Schemes Referenced to the Classic Scheme $[1 \quad -1]$

		$C_{p_{scheme/CFS}}$			
σ^2	$H(z)$	NLFS	CFS0	NLFS I	NLFS II
0.0005	$(1+z)/2$	1.9	5.4	5.5	7.3
0.0005	$1/6z^1+2/3+1/6z^{-1}$	1.9	4.9	6.3	6.8
0.005	$(1+z)/2$	2.2	5.3	5.7	6.9
0.005	$1/6z^1+2/3+1/6z^{-1}$	2.2	4.8	7.3	7.0

Parameters: threshold $= 0.08$. *The results depend on the parameters but the performance of the regularized schemes NLFS I and NLFS II is better than or equivalent to that of the CFS0. The performance of these methods relative to the classical regularized scheme CFS0 improves as the noise level increases. CFS0:* $D(z) = (1 - z^{-1}).H(z)$.

difference in performance between CFS0 and NLFS I-NLFS II seems to decrease with stronger regularization.

The best effect in noise reduction is obtained with local compensation: the same isolated peak detected by y_+ and y_- with the same localization. If regularization is introduced, the compensation is attenuated by averaging this detection over the neighborhood. This means that the NLFS I technique contradicts the principle holding in linear optimal detection filter and leading to the best SNR (difference of boxes). The compensation introduced by the NLFS II becomes negligible as regularization increases.

In conclusion, the performance of the NLFS I and NLFS II correlates with the energy of the regularized filter around its center.

5.4 Non-Gaussian Noises (No Regularization)

5.4.1 Multiplicative Noise

The multiplicative noise is defined as

$$J = I + \eta * I, \tag{62}$$

where I is the original image and η is uniformly distributed random noise with a mean of 0 and a variance v. The proposed scheme is still efficient for the derivation of a multiplicative noisy signal, while reducing the noise level (see Fig. 14). The performances $(C_{P_{NLFS}}/C_{P_{CFS}})$ are very similar to the Gaussian noise case; this ratio is about 2 for reasonable noise levels and more for high levels of noise.

5.4.2 Salt Noise

The NLFS is particularly efficient (see Fig. 15) for this type of noise since the underlying principle of the NLFS is designed to remove such isolated noise outcomes. The C_p criteria are not relevant for this particular noise ("binary" noise). Instead of C_p, the percentage of false detection P and the percentage of nondetected points ND are defined using the same procedure:

$$ND = \frac{1}{n_{E_R}} . \sum_{i,j \in \bar{E}_R} O_t(i,j), \tag{63}$$

$$P = \frac{1}{n_{E_R}} . \sum_{i,j \in \bar{E}_R} O_t(i,j), \tag{64}$$

where n_{E_R} is the number of edge points in the segmented reference image R_t and O_t is the segmented noisy image. Table 4 presents rough values of the gain in ND and P with respect to the classical derivative method. The range values for the threshold and the noise are set to obtain stable results with a reasonable number of edge points and noise points. The efficiency of the NLFS does not change outside this range.

5.5 Other Comparisons

All tests in this section are done on the *House* image and on a synthetic image containing simple patterns. As previously, ND and P are the performance indexes.

5.5.1 Schemes Involving the Same Neighborhood Size

To have a fair comparison between methods involving the same neighborhood size (S), we compare NLFS ($S = 5$) with a 2D CFS0 without regularization in the direction perpendicular to the detection (CFS05 with $S = 5$). Fig. 16a shows that for Gaussian noise, NLFS and CFS05 are equivalent, independent of the threshold, while both methods outperform CFS. This conclusion remains valid for any noise level. Fig. 16b shows that for salt noise, the performance of NLFS is superior to CFS05. As before, Fig. 16b illustrates that the behavior of the methods is similar whatever the threshold.

(a) (b) (c)

Fig. 13. Regularized schemes: the gradient modulus after local maxima and thresholding (0.08). (a) CFS0, (b) NLFS I, and (c) NLFS II. $House$ image + Gaussian noise $\sigma^2 = 0.005$, regularization filter $H(z) = 1/6z^1 + 2/3 + 1/6z^{-1}$.

(a) (b) (c)

Fig. 14. Speckle (multiplicative) noise: edge detection + segmentation (local maxima + threshold 0.08) on the *House* noisy image: (a) original image + speckle noise ($v = 0.001$), (b) CFS, and (c) NLFS detection.

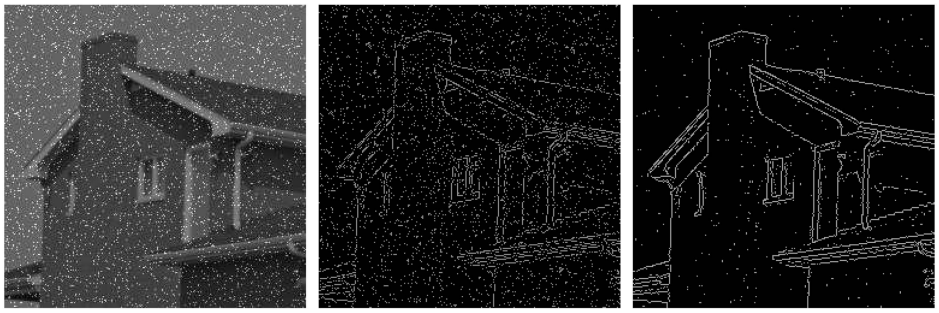

(a) (b) (c)

Fig. 15. Salt noise: edge detection + segmentation (local maxima + threshold 0.08) on the *House* noisy image: (a) original image + salt noise ($\text{density} = 0.1$), (b) CFS, and (c) NLFS detection.

TABLE 4
Performance of the NLFS Scheme in Terms of (Ratio of)
Percentage of False Detection P and Percentage of Nondetected Points ND

noise density	threshold	$ND_{CFS}\,/\,ND_{NLFS}$	P_{CFS}/P_{NLFS}
$[0.01; 0.1]$	$[0.08; 0.16]$	~ 5	~ 5

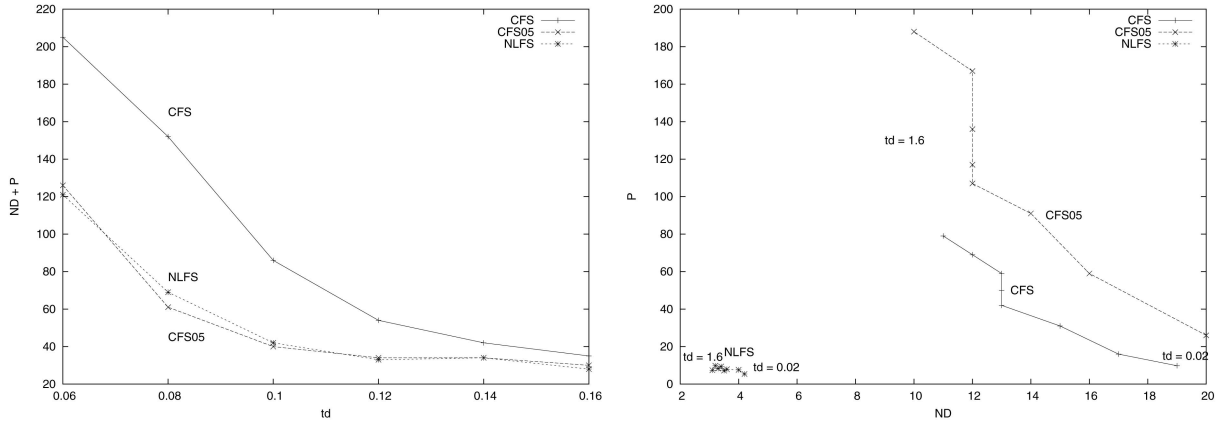

(a) (b)

Fig. 16. (a) Performance (measured by $ND + P$) of the methods with respect to the threshold (t_d) for the Gaussian noise (*House* image, $\sigma^2 = 0.0005$). (b) Performance of the methods measured by ND and P for the salt noise (*House* image, $density = 0.05$) for various thresholds t_d.

In the case of synthetic images containing ideal edges, even for Gaussian noise, NLFS greatly outperforms CFS05 and CFS. For example, with a Gaussian noise level $\sigma^2 = 0.0005$ and a threshold $t_d = 0.1$, we measured $(ND; P)$: $(5.9; 116)_{CFS}, (44; 59)_{CFS05}, (0.29; 4.2)_{NLFS}$, which illustrates the good localization ability of NLFS.

TABLE 5
Performance (ND, P) of Some Nonlinear Edge Detection Schemes
(Image *House*, $t_d = 0.1$, $\sigma^2 = 0.0005$ for the Gaussian Noise, $Density = 0.05$ for the Salt Noise

method		Median+CFS	Median+CFS05	Hwang-Haddad	NLFS	Median+NLFS
neighborhood size		7	9	11	5	9
gaussian noise	*ND*	15	17	21	16	15
	P	19	16	29	28	17
salt noise	*ND*	5.8	6.9	6.7	3.8	6.1
	P	14	17	16	7.9	9.2

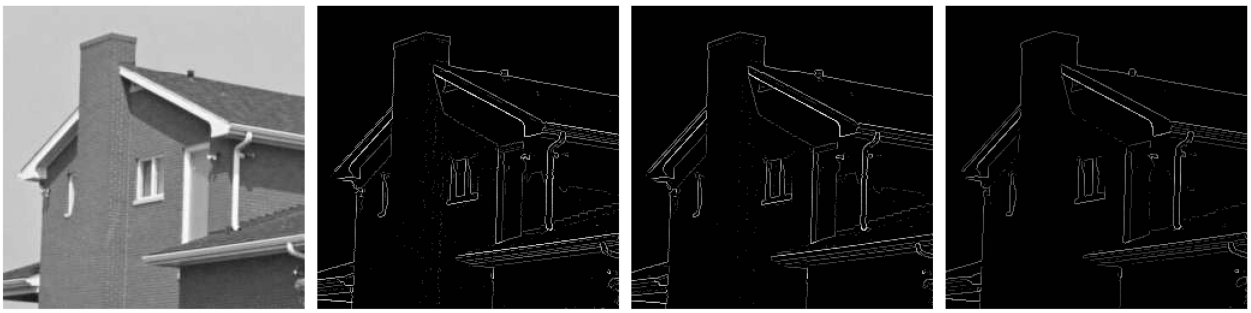

(a) (b) (c) (d)

Fig. 17. The *House* image: the gradient modulus after local maxima and thresholding (0.08). (a) Original image, (b) CFS detection, (c) NLFS detection, and (d) CFS0 reference detection (regularized).

5.5.2 Other Nonlinear Approaches

In this section, we propose to compare NLFS to other nonlinear methods. As stated in Section 1, very few nonlinear methods are specifically designed for edge detection. Considering only the methods comparable in complexity, we chose to compare NLFS with the scheme proposed by Hwang and Haddad [19] and with the commonly used technique that involves median filter followed by derivative: $\mathrm{Median} + \mathrm{CFS}$, $\mathrm{Median} + \mathrm{CFS05}$, and $\mathrm{Median} + \mathrm{NLFS}$. Table 5 presents the results obtained on the *House* image with Gaussian and salt noise. For the Gaussian noise, Median+CFS, Median+CFS05, and Median+NLFS produce the same results, while the (median-based version of) Hwang-Haddad method is not adapted to Gaussian noise. NLFS result is a slightly worse than the best methods (see Table 5) but it is the least complex scheme involving a 5-pixel neighborhood. However, once more, NLFS shows its efficiency when the image is corrupted by salt noise.

6 Natural Images

6.1 Sharp Images

The CFS0 on an original image is equivalent to the CFS applied on the original image convolved by the mask $[1\ 1; 1\ 1]/4$. Thus, the CFS0 corresponds to the narrowest filter among the family of derivative filters (Canny, Canny-Deriche, Shen and Castan, and Demigny, ...). This means that the CFS0 can be used for comparisons on sharp images. Another asymmetric regularization filter can be used to further smooth the derivative filter. Finally, the performance of NLFS against other kinds of noise can be evaluated.

Fig. 17 presents the detection (no threshold) on the *House* image. The detection by the NLFS can be compared to the CFS result and to the reference image obtained by CFS0. The edges are well detected using the NLFS except for the very thin edges (width 1 pixel). The roof is better detected with the NLFS than with the simple derivative scheme CFS.

Fig. 18 contains edges and thin textures. While the noise is slightly reduced, the textures are differently detected with NLFS than with linear approaches. Due to the localization inside the lighter object, patterns can be better isolated. Fig. 19 shows an example where the patterns seem easier to identify or separate. Nevertheless, some vertical thin lines are underdetected, as on the right of the visible hand. Fig 20 shows the efficiency of the NLFS scheme in removing noise similar to salt noise. Fig. 21 depicts an original image and its hand segmentation from the Berkeley database [24]. The results of the derivative schemes can be compared to this human reference. In the example, the tendency of the NLFS to underdetect thin edges (width of 1 pixel) can be considered to be a good property for human segmentation.

6.2 Degraded Images

In general, as confirmed by the results in the previous section, the simple derivative schemes work well on sharp images with homogeneous patterns (in luminance). Fig. 22 depicts the improvement in detection of the NLFS compared to the classical derivative method. It should be noted that the white lines of the ground are represented by one pixel in the NLFS detection. The result using CFS0 shows that regularization is needed to improve the detection of the object in the background. Two examples of regularization are carried out and the results are presented in Figs. 23 and 24. The regularization $H(z) = \sum_{k=-7}^{7} e^{-|k|} z^k$ is selected to avoid delocalization due to mutual influence [15]. This figure shows that regularization does not delocalize the edges in any of the schemes. Due to the equivalent regularization power of the NLFS schemes, the images created by the NLFS schemes contain slightly fewer noise points.

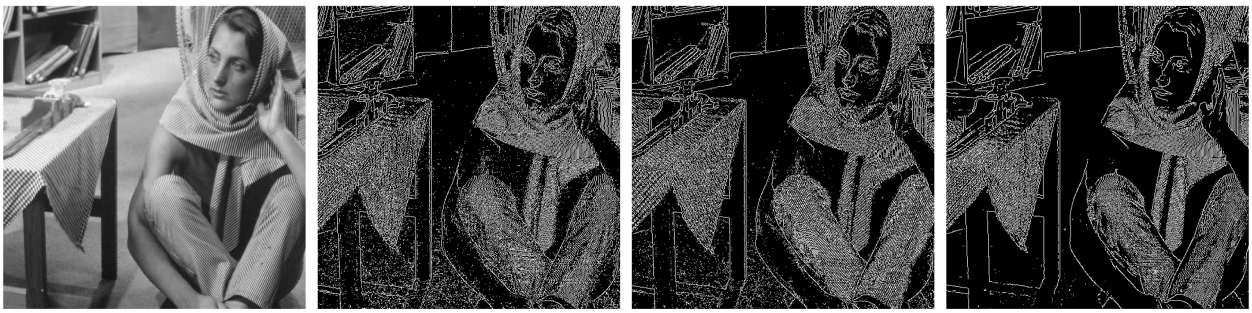

(a) (b) (c) (d)

Fig. 18. Segmentation of the Barbara image (threshold 0.04). (a) Original image, (b) CFS detection, (c) NLFS detection, and (d) CFS0 reference detection (regularized).

7 Conclusion

A new nonlinear scheme allowing the detection and univocal localization of edges with noise cancellation has been proposed. The noise cancellation effect is a beneficial property for an edge detector, since such a result is generally only obtained by linear regularization. It was demonstrated in [15] that this regularization generally induces delocalization for neighboring edges (a regularization filter should have a profile of $e^{-\alpha|x|}$ to avoid delocalization by mutual influence). The new scheme (NLFS) combines good localization, SNR improvement, robustness against mutual-edge influence, and a very low computational cost (similar to the simple discrete derivative method).

We compared the proposed scheme with the classical derivative scheme and the narrowest regularization scheme corresponding to the classical filters (such as the Canny, Canny-Deriche, Shen and Castan methods, ...). Without regularization, this very simple scheme can match the performance of regularized edge detectors for sharp images. The gain brought by this scheme can attain $4dB$ and the noise in the edge image is lower than that of the original image. Moreover, the edge is systematically localized inside the form (or outside), and this deterministic property can be useful for dimensional measurement and pattern recognition (thin textures and lines). A comparison of NLFS to other simple nonlinear edge detection schemes illustrates its simplicity and efficiency.

The method cannot remove the salt-and-pepper noise in the same operation. However, the scheme is efficient for many kinds of noise, including additive Gaussian white noise, salt or pepper noise, multiplicative noise, or any combination of these.

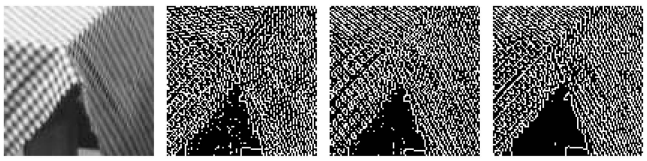

(a) (b) (c) (d)

Fig. 19. Zoom-in of the middle-left part of Fig. 18. (a) Original image, (b) CFS detection, (c) NLFS detection, and (d) CFS0 reference detection (regularized).

Since the scheme is fundamentally 1D, one-pixel width (along vertical or horizontal direction) lines with positive and negative contrast cannot be detected in the same operation. Depending on the application, the nondetection of these thin lines (1 pixel) can be seen as a positive property (in the case of human detection, for example) or as a problem (in detecting targets for robotic navigation). However, thin lines in 1D more often correspond to noise than to signal. These specific types of information should be detected by model-adapted detectors (see, for example, [6]).

The NLFS scheme can incorporate regularization in two ways, since it is nonlinear (NLFS and NLFS II). As in the classical scheme, this regularization can be chosen to avoid delocalization by mutual influence. More investigations are necessary, but it appears that NLFS I is more appropriate to Gaussian-like noise and NLFS II is very efficient for filtering impulse noise. In general, the gain brought by NLFS decreases as the regularization increases since the NLFS principle is based on local (around the center of the detection) compensation of the noise detection.

Future work will focus on the extension of this scheme and the definition of other elementary filters (F_+ and F_-: asymmetric and/or directly defined in 2D) to improve the performance of the NLFS.

Appendix

A.1 Signal-to-Noise Ratio

A.1.1 Signal Definition

Let us consider the noisy signal $s_k = A.H_k + n_k$, where $H_k = 1$ if $k \geq 0$, 0 elsewhere, and n_k is an outcome of the stochastic variable $\mathcal{N}_k$ denoting a Gaussian white noise of 0 mean and standard deviation σ.

A.1.2 Signal Output

Applying the NLFS on the signal s_k with the filter $f_+ = [\underline{1} - 1]$, we obtain the response $y = y_+ + y_-$:

$$\begin{cases} y_{+,k} = T[s_k - s_{k-1}] \\ y_{-,k} = -T[-(s_{k+1} - s_k)] \end{cases} \tag{65}$$

at $k = 0$ and introducing the noise and the edge model,

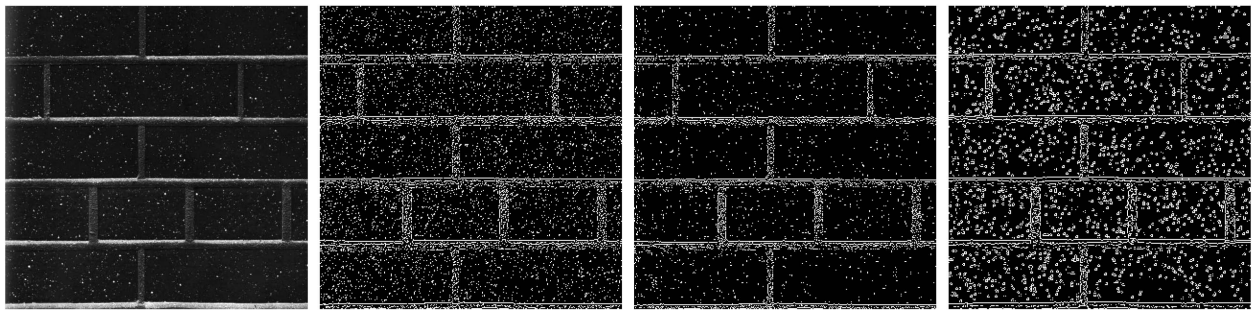

(a) (b) (c) (d)

Fig. 20. Segmentation of the brick wall image (Brodatz collection, image *D25*, threshold 0.04). (a) Original image, (b) CFS detection, (c) NLFS detection, and (d) CFS0 reference detection (regularized).

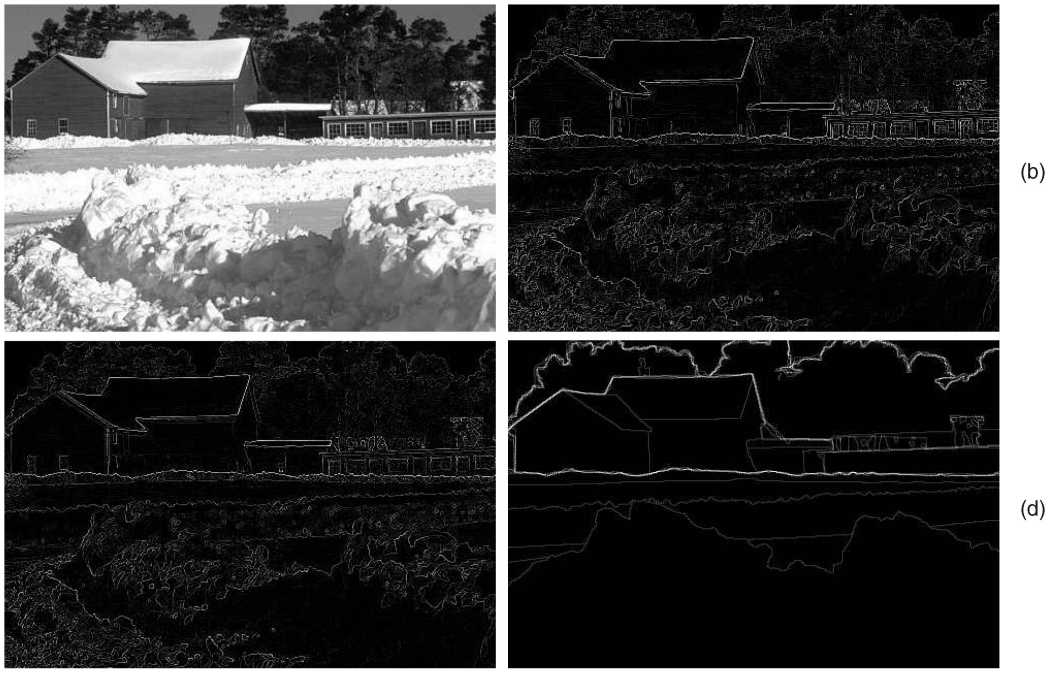

(a) (b) (c) (d)

Fig. 21. An image and its hand segmentation from the Berkeley database [24]. (a) Original image, (b) CFS detection, (c) NLFS detection, and (d) hand segmentation. The underdetection of thin lines by the NLFS agrees with the hand detection.

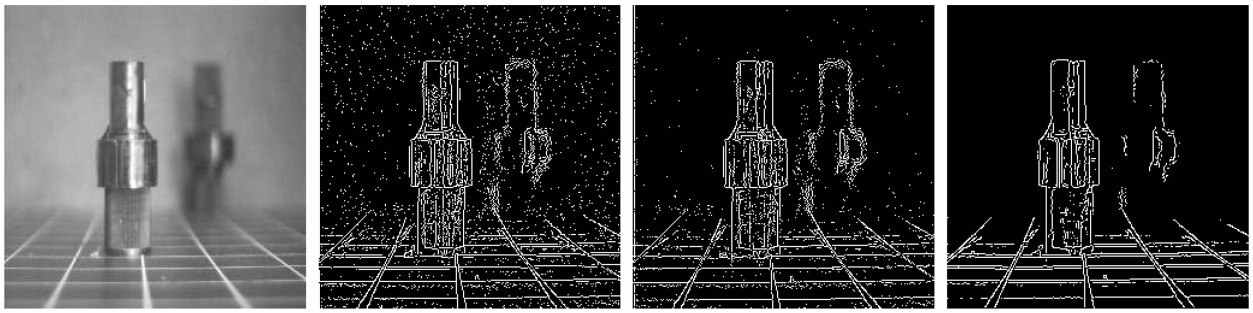

(a) (b) (c) (d)

Fig. 22. The "depth" image. Detection + modulus threshold 0.03. (a) Original image, (b) CFS detection, (c) NLFS detection, and (d) CFS0 detection (regularized).

$$\begin{cases} y_{+,0} = T[(A+n_0)-(0+n_{-1})], \\ y_{-,0} = -T[-((A+n_1)-(A+n_0))], \end{cases} \tag{66}$$

and then $y_0 = T[A+n_0-n_{-1})] - T[-n_1+n_0]$. In the following, the noise level is supposed to be weak compared to the amplitude A ($\sigma \ll A$). If it is not the case, the effect of the threshold will depend on the amplitude A: Experimental results show that the properties are close to the classical scheme ones. Now $y_0 \approx A + n_0 - n_{-1} - T[-n_1+n_0]$, which can be written as

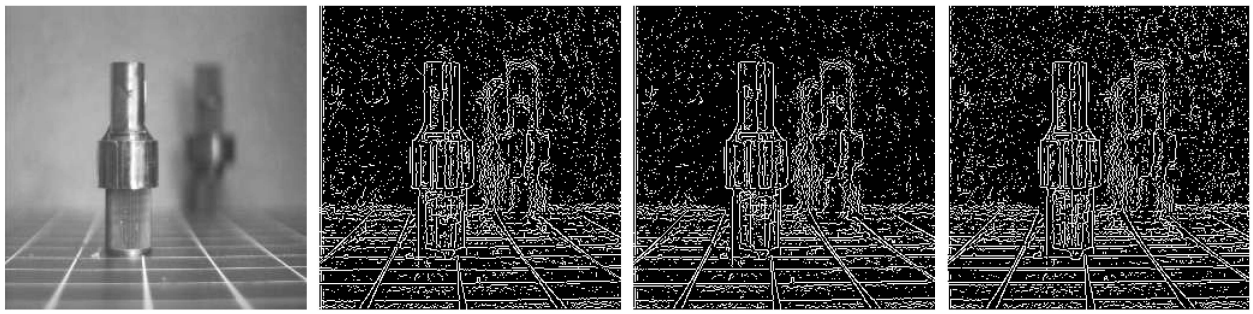

(a) (b) (c) (d)

Fig. 23. The "depth" image. Detection + modulus threshold 0.01 (low threshold to observe the noise reduction). (a) Original image, (b) NLFS I detection, (c) NLFS II detection, and (d) CFS regularized detection. $H(z) = 1/6z^1 + 2/3 + 1/6z^{-1}$.

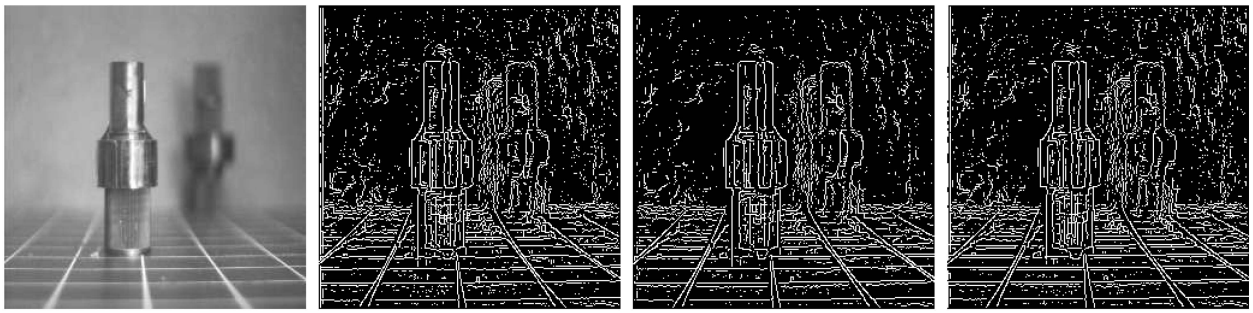

(a) (b) (c) (d)

Fig. 24. The "depth" image. Detection + modulus threshold 0.006 (low threshold to observe the noise reduction). (a) Original image, (b) NLFS I detection, (c) NLFS II detection, and (d) CFS regularized detection. $H(z) = \sum_{k=-7}^{7} e^{-|k|} z^k$.

$$\begin{cases} y_0 = A + n_1 - n_{-1} & \text{if } n_1 < n_0, \\ y_0 = A + n_0 - n_{-1} & \text{if } n_1 \geq n_0. \end{cases} \tag{67}$$

The energy of the noisy signal $\mathcal{Y}_0$, a random process, is given by

$$\begin{aligned} E\{\mathcal{Y}_0^2\} = E\{(A + \mathcal{N}_1 - \mathcal{N}_{-1})^2 \mid n_1 < \mathcal{N}_0\} \\ + E\{(A + \mathcal{N}_0 - \mathcal{N}_{-1})^2 \mid n_0 \leq \mathcal{N}_1\}, \end{aligned} \tag{68}$$

seeing $\mathcal{N}_1, \mathcal{N}_0, \mathcal{N}_{-1}$ are random variables:

$$\begin{aligned} E\{\mathcal{Y}_0^2\} = A^2 + 2A.(E\{(\mathcal{N}_1 - \mathcal{N}_{-1}) \mid n_1 < \mathcal{N}_0\} \\ + E\{(\mathcal{N}_0 - \mathcal{N}_{-1}) \mid n_0 \leq \mathcal{N}_1\}) \end{aligned} \tag{69}$$

$$+ E\{(\mathcal{N}_1 - \mathcal{N}_{-1})^2 \mid n_1 < \mathcal{N}_0\} + E\{(\mathcal{N}_0 - \mathcal{N}_{-1})^2 | n_0 \leq \mathcal{N}_1\}. \tag{70}$$

Considering the terms of the first case $(n_1 - n_{-1})$, we have:

$$P(n_{-1}) = \frac{1}{\sigma\sqrt{2\pi}} e^{\frac{-n_{-1}^2}{2\sigma^2}}, \tag{71}$$

$$P(n_1, n_1 < \mathcal{N}_0) = P(n_1).P(n_1 < \mathcal{N}_0) \tag{72}$$

$$= P(n_1). \int_{n_1}^{\infty} P(n_0) dn_0 \tag{73}$$

$$= \frac{1}{\sigma\sqrt{2\pi}} e^{\frac{-n_1^2}{2\sigma^2}}. \frac{1}{2}\left[1 - erf\left(\frac{\sqrt{2}}{2\sigma} n_1\right)\right]. \tag{74}$$

Defining the variable $\mathcal{M}$ as $\mathcal{M} = \mathcal{N}_1 - \mathcal{N}_{-1} \mid n_1 < \mathcal{N}_0$, the density probability $P_{\mathcal{M}}$ is:

$$P_{\mathcal{M}}(m) = \int_{-\infty}^{\infty} P(n_1, n_1 < \mathcal{N}_0).P(n_1 - m) dn_1 \tag{75}$$

$$= \int_{-\infty}^{\infty} P(n_1).P(n_1 - m) dn_1 \int_{n_1}^{\infty} P(n_0) dn_0. \tag{76}$$

We can deduce:

$$E\{(\mathcal{N}_1 - \mathcal{N}_{-1}) \mid \mathcal{N}_1 < n_0\} = \int_{-\infty}^{\infty} m P_{\mathcal{M}}(m) dm = -\frac{1}{2\sqrt{\pi}}\sigma \tag{77}$$

and

$$E\{(\mathcal{N}_1 - \mathcal{N}_{-1})^2 \mid \mathcal{N}_1 < n_0\} = \int_{-\infty}^{\infty} m^2 P_{\mathcal{M}}(m) dm = \sigma^2. \tag{78}$$

The second case $(n_0 - n_{-1})$ is identical. It follows that

$$E\{\mathcal{Y}_0^2\} = A^2 - A.\frac{2}{\sqrt{\pi}}.\sigma + 2\sigma^2 \quad \text{if } \sigma \ll A. \tag{79}$$

A.1.3 Noise Output

For the noise component, the detection leads to:

$$\begin{cases} y_{+,k} = T[s_k - s_{k-1}] \\ y_{-,k} = -T[-(s_{k+1} - s_k)] \end{cases} \tag{80}$$

or $(k \neq \{-1, 0, 1\})$:

$$\begin{cases} y_{+,k} = T[n_k - n_{k-1}] \\ y_{-,k} = -T[-(n_{k+1} - n_k)]. \end{cases} \tag{81}$$

Developing the different cases, we obtain for $y_k = y_{+,k} + y_{-,k}$:

$$\begin{cases} y_k = n_{k+1} - n_{k-1} & \text{if } n_k > n_{k-1} \text{ and } n_k > n_{k+1}, & (a) \\ y_k = n_k - n_{k-1} & \text{if } n_k > n_{k-1} \text{ and } n_k \leq_{k+1}, & (b) \\ y_k = n_{k+1} - n_k & \text{if } n_k \leq n_{k-1} \text{ and } n_k > n_{k+1}, & (c) \\ y_k = 0 & \text{if } n_k \leq n_{k-1} \text{ and } n_k \leq n_{k+1}. & (d) \end{cases} \tag{82}$$

We deduce the corresponding density probabilities:

$$\begin{aligned} P_a(y) &= \int_{-\infty}^{\infty} P_k(x)dx \left[\int_{-\infty}^{x} P_{k+1}(u)P_{k-1}(u - y_{>0})du \right. \\ &\quad \left. + \int_{x}^{\infty} P_{k+1}(u)P_{k-1}(u - y_{<0})du \right] \\ &= \int_{-\infty}^{\infty} P_k(x)dx \int_{-\infty}^{x} P_{k+1}(u)P_{k-1}(u - |y|)du \\ P_b(y) &= \int_{-\infty}^{\infty} P_{k+1}(x)dx \int_{-\infty}^{x} P_k(u)P_{k-1}(u - y)du \\ P_c(y) &= \int_{-\infty}^{\infty} P_{k-1}(x)dx \int_{x}^{\infty} P_{k+1}(u)P_k(u - y)du \end{aligned}$$

The two moments are then calculated by: $E\{Y_k\} = \int_{-\infty}^{\infty} yP(y)dy$ and $E\{Y_k^2\} = \int_{-\infty}^{\infty} y^2P(y)dy$. We obtain the following results:

y_k	a	b	c
$E\{Y_k\}$	0	$\frac{1}{2\sqrt{\pi}}\sigma$	$-\frac{1}{2\sqrt{\pi}}\sigma$
$E\{Y_k^2\}$	$\frac{\pi}{8}\sigma^2$	$\frac{\pi}{16}\sigma^2$	$\frac{\pi}{16}\sigma^2$

Finally, $E\{Y_k\} = 0$ and $E\{Y_k^2\} = \frac{\pi}{4}\sigma^2 \approx 0.785\sigma^2$. This means that, while a derivative operation is performed, the centered noise of variance σ^2 is reduced to a variance $0.785\sigma^2$ (centered noise).

A.1.4 Theoretical SNR

The theoretical SNR is defined by:

$$SNR = \frac{\text{noisy signal power average } - \text{ noise power average}}{\text{noise power average}} \tag{83}$$

with the previous results:

$$SNR = \frac{\left(A^2 - A.\frac{2}{\sqrt{\pi}}.\sigma + 2\sigma^2\right) - \frac{\pi}{4}\sigma^2}{\frac{\pi}{4}\sigma^2} \tag{84}$$

$$= \frac{4}{\pi}.\frac{A^2}{\sigma^2}\left(1 - \frac{2}{\sqrt{\pi}}.\frac{\sigma}{A} + \frac{8-\pi}{4}.\frac{\sigma^2}{A^2}\right). \tag{85}$$

Seeing the condition for the signal power average evaluation ($\sigma \ll A$), we have $\frac{2}{\sqrt{\pi}}.\frac{\sigma}{A} \gg \frac{8-\pi}{4}.\frac{\sigma^2}{A^2}$ and:

$$SNR \approx \frac{4}{\pi}.\frac{A^2}{\sigma^2}\left(1 - \frac{2}{\sqrt{\pi}}.\frac{\sigma}{A}\right), \tag{86}$$

and then $SNR_{\max} \approx \frac{4}{\pi}.\frac{A^2}{\sigma^2} \approx 1.27\frac{A^2}{\sigma^2}$.

A.1.5 Comparison with the Theoretical SNR for the Classical Scheme

$$SNR_{CFS,CFS0} = \frac{1}{2}.\frac{A^2}{\sigma^2}. \tag{87}$$

We can now establish the gain of the basic NLFS scheme in SNR:

$$G_{SNR} = \frac{8}{\pi}\left(1 - \frac{2}{\sqrt{\pi}}.\frac{\sigma}{A}\right) \quad \text{if } \sigma \ll A \tag{88}$$

and the maximum gain $G_{SNR_{\max}} = \frac{8}{\pi} \approx 2.55$ if $\sigma \ll A$.

A.2 Matlab-Octave-... Code of NLFS

```
%- - - - - - - - - - - - algo. NLFS - - - - - - - - - - - -
% input I: image, size M × N
% outputs gm, gh, gv: gradient modulus and
components, size M × N
function [gm, gh, gv] = algoNLFS(I);

% no optimization
dph = threshold(conv2(I, [0 1 -1], 'same'), 0);
dnh = -threshold(-conv2(I, [1 -1 0], 'same'),
      0);
gh = dph + dnh; % horizontal component of the
     gradient
dpv = threshold(conv2(I, [0; 1; -1], 'same'),
      0);
dnv = -threshold(-conv2(I, [1; -1; 0], 'same'),
      0);
gv = dpv + dnv; % vertical component of the
     gradient
gm = sqrt(gh.*gh + gv.*gv);
%- - - - - - - - - - end algo. NLFS - - - - - - - - - -

%- - - - - - - - - - - - - threshold - - - - - - - - - - -
% s: signal or image, T: threshold (0 in this
     work)
function st = threshold(s, T)
for i=1:size(s,1)
   for j=1:size(s,2)
      if (s(i,j) <= t)   st(i,j) = 0;
      else               st(i,j) = s(i,j);
```

```
      end
   end
end
%- - - - - - - - - - end threshold - - - - - - - - -
```

ACKNOWLEDGMENTS

The authors thank the reviewers and the Editor for their invaluable comments and suggestions. They also thank Prof. Hamed Sari-Sarraf for his help.

REFERENCES

[1] J.W. Modestino and R.W. Fries, "Edge Detection in Noisy Images Using Recursive Digital Filtering," *Computer Graphics and Image Processing,* vol. 6, pp. 409-433, 1977.
[2] J.-O. Eklundh, T. Elfving, and S. Nyberg, "Edge Detection Using the Marr-Hildreth Operator with Different Sizes," *Proc. IEEE Int'l Conf. Pattern Recognition,* vol. 6, pp. 1109-1112, 1982.
[3] P. Bolon, A. Raji, P. Lambert, and M. Mouhoub, "Recursive Median Filters—Application to Noise Reduction and Edge Detection" *Proc. Fifth European Signal Processing Conf.,* pp. 813-816, Sept. 1990.
[4] V. Torre and T.A. Poggio, "On Edge Detection," *IEEE Trans. Pattern Analysis and Machine Intelligence,* vol. 8, no. 2, pp. 147-163, Mar. 1986.
[5] J. Canny, "A Computational Approach to Edge Detection," *IEEE Trans. Pattern Analysis and Machine Intelligence,* vol. 8, no. 6, pp. 679-698, Nov. 1986.
[6] D. Ziou, "Line Detection Using Optimal IRR Filter," *Pattern Recognition,* vol. 24, no. 6, pp. 465-478, 1991.
[7] R. Deriche, "Using Canny's Criteria to Derive a Recursively Implemented Optimal Edge Detector," *Int'l J. Computer Vision,* vol. 1, no. 2, pp. 167-187, May 1987.
[8] E. Bourennane, P. Gouton, M. Paindavoine, and F. Truchetet, "Generalization of Canny-Deriche Filter for Detection of Noisy Exponential Edge," *Signal Processing,* vol. 12, no. 10, pp. 1317-1328, Oct. 2002.
[9] M. Jacob and M. Unser, "Design of Steerable Filters for Feature Detection Using Canny-Like Criteria," *IEEE Trans. Pattern Analysis and Machine Intelligence,* vol. 26, no. 8, pp. 1007-1019, Aug. 2004.
[10] K.L. Boyer and S. Sarkar, "On the Localization Performance Measure and Optimal Edge Detection," *IEEE Trans. Pattern Analysis and Machine Intelligence,* vol. 16, no. 1, pp. 106-110, Jan. 1994.
[11] S. Kumar, S.H. Ong, S. Ranganath, and F.T. Chew, "A Luminance- and Contrast-Invariant Edge-Similarity Measure," *IEEE Trans. Pattern Analysis and Machine Intelligence,* vol. 28, no. 12, pp. 2042-2048, Dec. 2006.
[12] D. Demigny and T. Kamlé, "A Discrete Expression of Canny's Criteria for Step Edge Detector Performances Evaluation," *IEEE Trans. Pattern Analysis and Machine Intelligence,* vol. 19, no. 11, pp. 1199-1211, Nov. 1997.
[13] F. Truchetet, F. Nicolier, and O. Laligant, "Supixel Edge Detection for Dimensional Control by Artificial Vision," *J. Electronic Imaging,* vol. 10, no. 1, pp. 234-239, Jan. 2001.
[14] D. Demigny, "On Optimal Linear Filtering for Edge Detection," *IEEE Trans. Image Processing,* vol. 11, no. 7, pp. 728-737, July 2002.
[15] O. Laligant, F. Truchetet, and F. Mériaudeau, "Regularization Preserving Localization of Close Edges," *IEEE Signal Processing Letters,* vol. 14, no. 3, pp. 185-188, Mar. 2007.
[16] I. Pitas and A. Venetsanopoulos, "Nonlinear Mean Filters in Image Processing," *IEEE Trans. Acoustics, Speech, and Signal Processing,* vol. 34, no. 3, pp. 573-584, June 1986.
[17] A. Benazza-Benyahia, J.-C. Pesquet, and H. Krim, "A Nonlinear Diffusion-Based 3-Band Filter Bank," *IEEE Signal Processing Letters,* vol. 10, pp. 360-363, Dec. 2003.
[18] M.A. Schulze, "An Edge-Enhancing Nonlinear Filter for Reducing Multiplicative Noise," *Nonlinear Image Processing VIII,* pp. 46-56, SPIE, 1997.
[19] H. Hwang and R. Haddad, "Multilevel Nonlinear Filters for Edge Detection and Noisesuppression," *IEEE Trans. Signal Processing,* vol. 42, no. 2, pp. 249-258, Feb. 1994.
[20] I.E. Abdou and W.K. Pratt, "Quantitative Design and Evaluation of Enhancement/Thresholding Edge Detectors," *Proc. IEEE,* vol. 67, no. 5, pp. 753-763, May 1979.
[21] S. Tabbone and D. Ziou, "Subpixel Positioning of Edges for First and Second Order Operators," *Proc. Int'l Conf. Pattern Recognition,* pp. 655-658, 1992.
[22] K. Chen, "Adaptative Smoothing via Contextual and Local Discontinuities," *IEEE Trans. Pattern Analysis and Machine Intelligence,* vol. 27, no. 10, pp. 1552-1567, Oct. 2006.
[23] M. Petrou and J. Kitler, "Optimal Edge Detectors for Ramp Edges," *IEEE Trans. Pattern Analysis and Machine Intelligence,* vol. 13, no. 5, pp. 483-491, May 1991.
[24] D. Martin, C. Fowlkes, and J. Malik, "Learning to Detect Natural Image Boundaries Using Local Brightness, Color and Texture Cues," *IEEE Trans. Pattern Analysis and Machine Intelligence,* vol. 26, no. 1, pp. 530-549, May, 2004.

Olivier Laligant received the PhD degree from the Université de Bourgogne, France, in 1995. He is full professor in the Computing, Electronic, Imaging Department (Le2i) at the Université de Bourgogne, France. His research interests are focused on multiscale edge detection, merging of data, and wavelet transform.

Frédéric Truchetet received the master's degree in physics and the PhD degree in electronics from Dijon University, France, in 1973 and 1977, respectively. He was with Thomson-CSF for two years as a research engineer and is currently a full professor at Le2i, Laboratory of Electronic, Computer, and Imaging Sciences, Université de Bourgogne, France. His research interests are focused on image processing for artificial vision inspection and particularly on wavelet transforms, multiresolution edge detection, and image compression. He is a member of the IEEE.